Journal of Magnetic Resonance **145,** 24–36 (2000)
doi:10.1006/jmre.2000.2059, available online at http://www.idealibrary.com on IDEAL®

Quantitative Interpretation of Magnetization Transfer in Spoiled Gradient Echo MRI Sequences

John G. Sled and G. Bruce Pike

McConnell Brain Imaging Centre, Montréal Neurological Institute, McGill University, Montréal, Québec, Canada H3A 2B4

E-mail: jgsled@bic.mni.mcgill.ca, bruce@bic.mni.mcgill.ca

Received September 21, 1999; revised February 21, 2000

A method for analyzing general pulsed magnetization transfer (MT) experiments in which off-resonance saturation pulses are interleaved with on-resonance excitation pulses is presented. We apply this method to develop a steady-state signal equation for MT-weighted spoiled gradient echo sequences and consider approximations that facilitate its rapid computation. Using this equation, we assess various experimental designs for quantitatively imaging the fractional size of the restricted pool, cross-relaxation rate, and T_1 and T_2 relaxation times of the two pools in a binary spin bath system. From experiments on agar gel, this method is shown to reliably and accurately estimate the exchange and relaxation properties of a material in an imaging context, suggesting the feasibility of using this technique *in vivo.*

Key Words: **magnetization transfer; cross-relaxation; quantitative imaging; magnetic resonance imaging.**

1. INTRODUCTION

Magnetization transfer (MT) provides a form of contrast that allows one to indirectly observe ^{1}H atoms whose resonance is too short to be observed using conventional MR imaging. Initially developed for biological applications as an NMR experiment (*1*), MT contrast has since been incorporated into a variety of imaging techniques (*2–5*). Many of these use so-called magnetization transfer contrast ratios (MTR) to represent the signal change induced by MT. While MTR techniques are quantitative, the usefulness of these ratios is limited by their dependences on the specific details of the pulse sequence and imaging hardware (*6*). Furthermore, clinical limitations on power absorption preclude completely saturating the restricted pool so as to simplify the interpretation of the data (*1, 7*).

NMR experiments employing continuous-wave (CW) off-resonance irradiation to create MT contrast have been used to characterize a variety of materials in terms of their intrinsic relaxation properties (*8, 9*). These methods are based on a binary spin bath model (*10, 11*) in which protons belong to either a free pool ^1H_f, consisting primarily of hydrogen bound to water, and a restricted pool ^1H_r, consisting of hydrogen bound to larger molecules. The two pools are assumed to transfer magnetization either by chemical exchange or dipolar magnetic interaction (*12*).

A number of authors have proposed MT imaging techniques that yield intrinsic properties based on the binary spin bath model. Quesson *et al.* (*13, 14*) have described a technique similar to an NMR experiment (*15*) in which continuous-wave off-resonance irradiation is used to prepare the magnetization before performing conventional imaging. Lee and Dagher (*16*) proposed a similar technique with fewer measurements that yields only the fractional size of the restricted pool. An alternate technique, yielding all of the parameters of the binary spin bath model, described by Chai *et al.* (*17*) measures the approach to steady state for trains of binomial pulses of varying duty cycle and duration. Another method recently described by Gochberg *et al.* (*18*) saturates the restricted pool by successive inversions of the free pool so as to estimate the fractional size of the restricted pool and relaxation properties of the free pool.

The challenges of developing a clinical imaging technique that yields exchange and relaxation properties based on the binary spin bath model are threefold. First, one needs to forgo the use of continuous-wave irradiation, which is not widely available, and the large power deposition that is typical of NMR experiments. Second, sufficient data to constrain all aspects of the model need to be collected within a relatively short period, such as half an hour. And third, a computationally efficient model of the experiment is needed so that estimation of the model parameters at every voxel becomes feasible. Existing methods either do not meet all of these criteria or yield only a subset of the relaxation parameters.

In this work we describe a method for analyzing general pulsed MT experiments in which off-resonance saturation pulses are interleaved with on-resonance excitation (imaging) pulses. We apply this method to develop a signal equation for MT-weighted spoiled gradient echo sequences and consider approximations that facilitate its rapid computation. Using this equation, we assess various experimental designs for imaging the fractional size of the restricted pool, cross-relaxation rate, and T_1 and T_2 relaxation times of the two pools. In doing so, we demonstrate the feasibility of using conventional MT-

1090-7807/00 $35.00

weighted MRI pulse sequences to rapidly produce quantitative images of the exchange and relaxation properties within an object.

2. METHODS

2.1. Modeling Pulsed MT Sequences

We have employed a binary spin bath model to predict the behavior of materials in pulsed MT experiments. In this approach, the magnetization of the free pool is described by the Bloch equations while that of the restricted pool is modeled using the Redfield–Provotorov theory (*19*). A first-order rate constant governs exchange between the two pools.

For experiments on clinical scanners the timescale is short enough and the irradiation is weak enough compared to the main magnetic field B_0 that the Zeeman and dipolar terms in the Hamiltonian have their own associated temperatures. Expressed as five coupled differential equations the behavior of the magnetization is given by

$$\frac{dM_{x,\mathrm{f}}}{dt} = -\frac{M_{x,\mathrm{f}}}{T_{2,\mathrm{f}}} - \Delta M_{y,\mathrm{f}} - \mathrm{Im}(\omega_1) M_{z,\mathrm{f}} \quad [1]$$

$$\frac{dM_{y,\mathrm{f}}}{dt} = -\frac{M_{y,\mathrm{f}}}{T_{2,\mathrm{f}}} + \Delta M_{x,\mathrm{f}} + \mathrm{Re}(\omega_1) M_{z,\mathrm{f}} \quad [2]$$

$$\frac{dM_{z,\mathrm{f}}}{dt} = R_{1,\mathrm{f}}(M_{0,\mathrm{f}} - M_{z,\mathrm{f}}) - k_{\mathrm{f}} M_{z,\mathrm{f}} + k_{\mathrm{r}} M_{z,\mathrm{r}} + \mathrm{Im}(\omega_1) M_{x,\mathrm{f}} - \mathrm{Re}(\omega_1) M_{y,\mathrm{f}} \quad [3]$$

$$\frac{dM_{z,\mathrm{r}}}{dt} = R_{1,\mathrm{r}}(M_{0,\mathrm{r}} - M_{z,\mathrm{r}}) - k_{\mathrm{r}} M_{z,\mathrm{r}} + k_{\mathrm{f}} M_{z,\mathrm{f}} - W M_{z,\mathrm{r}} + W\beta' \quad [4]$$

$$\frac{d\beta'}{dt} = W\left(\frac{2\pi\Delta}{\mathrm{D}}\right)^2 (M_{z,\mathrm{r}} - \beta') - \frac{1}{T_{\mathrm{D}}}\beta', \quad [5]$$

where the subscripts f and r denote the free and restricted pools and the subscripts x, y, and z denote the various components of a magnetization vector. β is the inverse spin temperature associated with the dipolar order of the restricted pool. T_{D} is the dipolar relaxation time. $\omega_1 = \gamma B_1$, the excitation field strength, is complex and time varying for general pulses with a circularly polarized coil. The parameter D is related to the linewidth of the restricted pool (*19*); for a Gaussian lineshape this is given by $D^2 = 1/3T_{2,\mathrm{r}}^2$. By definition, $k_{\mathrm{r}} = k_{\mathrm{f}}/F$, where $F = M_{0,\mathrm{r}}/M_{0,\mathrm{f}}$ is the ratio of the pool sizes.

The transition rate W for the saturation of the restricted pool is given for CW experiments in the absence of B_0 field gradients by

$$W = \pi\omega_1^2 G(\Delta), \quad [6]$$

where G is the lineshape function for the restricted pool. When G is a Lorentzian, the behavior of the system approximates that of the Bloch equations for small $T_{2,\mathrm{r}}$ (*20*). Gaussian lineshapes have been found appropriate for solids and gels (*15*) as have super-Lorentzians for tissues (*21*). If the system is assumed to be in steady state then irradiation patterns more complex than a continuous wave can be accounted for by summing the transition rates of the various spectral components (*22, 23*).

For sufficiently short pulses the approximation that the magnetization of the restricted pool is constant during a repetition period of a pulse sequence may not be satisfactory. In such circumstances the transition rate will be time varying. Treating the restricted pool as a causal linear system, the lineshape can be interpreted as the real part of a complex susceptibility function from which the impulse response of the system is readily computed to be

$$g(t) = \frac{2}{\pi}\int_0^\infty G(\Delta)\cos(\Delta t)\, d\Delta, \quad t > 0. \quad [7]$$

Convolving this response function with the instantaneous irradiation power yields the time-varying transition rate

$$W(t) = \pi\omega_1^2(t) * g(t). \quad [8]$$

However, for shaped MT pulses with bandwidths narrow compared to the linewidth, the transition rate can be approximated as

$$W(t) = \pi\omega_1^2(t) G(\Delta), \quad [9]$$

where Δ is the center frequency of the off-resonance irradiation.

While we propose Eqs. [1]–[5] and [9] as an accurate model for describing pulsed MT experiments, in practice using these ordinary differential equations to estimate the parameters of the spin bath model from experimental data is computationally infeasible. Given that one needs to construct a series of experiments in order to completely characterize the binary spin bath model and that, due to the complexity the model, the process of estimation is inevitably iterative, one may need to numerically solve these equations upward of ten million times for an imaging protocol. In subsequent sections we describe a number of approximate solutions to these equations that lend themselves to rapid computation. These approximations were made in view of the experiments that we describe briefly in the following section.

2.2. Outline of Experiments

We have validated our signal equation using two acquisition strategies and various concentrations of agar gel, a material whose MT properties have been well characterized (*15*) by the

TABLE 1
Model Parameters for 2, 4, and 8% Agar Based on CW Experiments Reported by Henkelman *et al.* (15)

	2% agar	4% agar	8% agar
k_f	$0.9 \pm 0.1\ s^{-1}$	$1.8 \pm 0.2\ s^{-1}$	$3.9 \pm 0.5\ s^{-1}$
F	0.0051 ± 0.001	0.011 ± 0.002	0.022 ± 0.004
$R_{1,f}$	$0.51 \pm 0.07\ s^{-1}$	$0.70 \pm 0.10\ s^{-1}$	$1.08 \pm 0.16\ s^{-1}$
$R_{1,r}$	$1 \pm 1\ s^{-1}$	$1 \pm 1\ s^{-1}$	$1 \pm 1\ s^{-1}$
$T_{2,f}$	63 ± 8 ms	32 ± 4 ms	16 ± 2 ms
$T_{2,r}$	$12.9 \pm 0.1\ \mu s$	$12.9 \pm 0.1\ \mu s$	$12.9 \pm 0.1\ \mu s$

Note. The corresponding values of R_1^{obs} were 0.49 ± 0.02, 0.68 ± 0.03, and $1.14 \pm 0.05\ s^{-1}$, respectively.

binary spin bath model with a Gaussian lineshape for the restricted component and neglecting the dipolar reservoir. The model parameters reported by Henkelman *et al.* (*15*) at 1.5 T for 2, 4, and 8% agar are given in Table 1.

We performed two types of experiments on agar gels. The first, which we call a magnetization transfer prepared (MTP) sequence, consists of a train of shaped off-resonance pulses that drive the system into steady state after which the z magnetization of the free pool is measured using a 90° pulse. Phase cycling (*24*) rather than RF spoiling is used to select the FID of the 90° pulse making this experiment analogous to the NMR experiments described in (*15*), in which a period of continuous-wave irradiation was used to drive the system into steady state before measurement with a 90° pulse.

The second type of experiment, a spoiled gradient echo sequence (MTSPGR), has an MT pulse followed by a slice-selective low-angle excitation pulse and readout at every repetition. RF spoiling and crusher gradients are used to disperse transverse magnetization produced by the MT pulses and prevent the formation of stimulated echoes. When comparing the two types of sequences we refer to the repetition period for the MT pulse (T_{MT}) which for the MTSPGR sequence is same as the repetition time of the excitation (TR).

2.3. A Signal Equation for Pulsed MT Sequences

One can predict the outcome of a pulsed MT experiment by numerically solving the ordinary differential Eqs. [1]–[5] over a time interval long enough for a steady state to establish. We use this method as the standard to evaluate various approximate signal equations. Following the derivation of (*25*) we decomposed the pulsed sequences into a number of stages which have simple exact or approximate solutions to the ODEs. Concatenating these solutions together and solving algebraically for the magnetization in steady state yields a signal equation that can be rapidly computed.

Three cases having simple solutions to the differential equations are those of instantaneous pulsed excitation, continuous-wave excitation, and free precession. These solutions can be combined in a number of ways. For example, concatenating the solution for a period of continuous-wave excitation followed by a period without saturation yields the responses to an off-resonance rectangular pulse. Furthermore, different approximate solutions can be used for the two pools.

Since the behavior of the free pool near resonance tends to be complicated, neither a continuous-wave nor a rectangular pulse approximation is satisfactory. Instead we modeled the effect of an MT pulse on the free pool as an instantaneous fractional saturation of the longitudinal magnetization. This saturation fraction is computed by simulation of the Bloch equations taking into account the pulse envelope and $T_{2,f}$ decay but neglecting exchange with the restricted pool and $R_{1,f}$ recovery. Neglecting these terms is compensated for by including $R_{1,f}$ recovery and exchange in the adjacent stages of the sequence. This approach is taken to uncouple $T_{2,f}$ from $R_{1,f}$ and k_f thus limiting the number of parameters that the saturation fraction depends on. With the saturation fraction only depending on $T_{2,f}$ for a particular pulse envelope, these fractions which are relatively expensive to compute are computed in advance and reused in subsequent calculations.

We considered two models for the restricted pool, one in which it experiences continuous-wave excitation of equivalent average power and another in which the MT pulse is replaced by a rectangular pulse having equivalent average power and a width equal to the full width at half-maximum of the instantaneous pulse power $\omega_1^2(t)$. While we investigated taking into account the bandwidth of the shaped pulses in the former model, we found this correction to be negligible for these experiments.

An additional variation we considered was to neglect the dipolar term in the Hamiltonian. Altogether, this gave us four models to evaluate, two variants of the signal equation each with and without the dipolar term. For each of these models the excitation pulse was incorporated as an additional fractional saturation of the free pool and, due to its lower power, was not considered for the bound pool. The formulas for the steady-state magnetization are given in the Appendix.

2.4. Numerical Simulations

Numerical simulations were used to investigate two aspects of our methodology. The first was to determine how closely the various signal equations predict the results of the numerical simulations, which we assume to be correct. The second was to determine which pulse sequence designs yield the best predictions. While we did not exhaustively pursue the latter, we looked at the five pulse sequences for which experimental data were also collected. Simulations with and without the dipolar terms were made for each of three materials having the properties of 2, 4, and 8% agar given in Table 1. These simulations were also used to assess bias in the parameter estimation technique described in Section 2.6.

The numerical simulations were computed using a standard ODE solver in which the simulation was stopped when the

TABLE 2
Summary of Experiments Using Spatial Encoding of MT Offset Frequencies

Experiment	Type	TR	Pulse duration	MT pulse angles			Excitation angle
I	MTP	15 ms	10.24 ms	219°	438°	657°	90°
II	MTP	50 ms	30.72 ms	693°	1386°	2079°	90°
III	MTSPGR	50 ms	10.24 ms	400°	800°	1200°	10°
IV	MTSPGR	50 ms	30.72 ms	693°	1386°	2079°	10°
V	MTSPGR	25 ms	10.24 ms	283°	566°	849°	7°

difference in magnetization at the readout time differed by less than 0.05% from that at the previous repetition. Spoiling was modeled by setting the transverse components of the magnetization to zero after each MT pulse.

2.5. Experimental Validation

The MTP sequences consisted of a 7.7-s train of MT pulses (for $T_{MT} = 15$ ms this corresponds to 512 pulses) followed by a 90° on-resonance excitation pulse and gradient echo readout with TE = 4 ms. Based on numerical simulations 7.7 s was sufficient to establish steady state for these experiments. The MT pulses used were Hanning windowed Gaussians with duration 10.24 or 30.72 ms (bandwidth 200 and 67 Hz) whose offset frequency and power could be varied. Phase cycling of the 90° pulse was used to separate its FID from coherences generated by the MT pulses.

The MTSPGR experiments consisted of a gradient echo sequence with TE = 4 ms and TR = T_{MT} either 50 or 25 ms. Excitation pulse angles of 10° and 7° were chosen for the two cases based on the MT contrast relative to noise determined by numerical simulation. A combination of strong crushing gradients and RF spoiling (*26*) was used to eliminate any residual transverse magnetization between repetitions. On the basis of numerical simulation, a period of 12.8 s of initial pulsing was determined to be sufficient to establish steady state and was used in all MTSPGR studies before data were acquired.

The agar gels for these experiments were prepared in 1-liter bottles, 16 cm high. This allowed for a spectrum of offset frequencies to be tested in a single experiment by employing a linear field gradient (*27*) along the cylinder axis during the MT pulses. Since in practice we were interested in a logarithmic series of frequency offsets, data were acquired in three stages, capturing a range from zero to 1, 10, and 100 kHz, respectively.

The raw data from these experiments are biased by a combination of nonuniform coil sensitivity and nonuniform excitation (B_1) field strength (*28*), the latter of which affects both the MT and the excitation pulses. Rather than model the two effects we chose to collect an additional gradient echo scan without MT pulses which we used to estimate a smooth nonuniformity field (*29*) and normalize the intensity of the MTSPGR data. This approach compensates for reception sensitivity variations as well as variations in the excitation pulses. In addition, we measured the main magnetic field variations (B_0) using a phase difference imaging technique (*30*) and corrected the offset frequencies of the MT pulses accordingly.

A summary of the various experiments conducted using spatial encoding of MT offset frequency is given in Table 2. Each experiment was repeated for three different MT pulse angles (powers). The average irradiation power corresponding to each of the three pulses is the same for each type of experiment.

As an additional experiment we used a series of MTSPGR images to compute parameter images for the various material properties. For this experiment we used pulse sequences IV and V with only the low- and high-power pulses. Each experiment was conducted for 16 offset frequencies ranging from 800 Hz to 80 kHz from resonance. While these experiments were normalized using a scan without MT pulses as before, we also measured B_1 field strength using a modified stimulated echo pulse sequence (*31*) and corrected the MT pulse power at each voxel. Images were made for a transverse section of the three gel bottles along with a bottle of 254 μM $MnCl_2$ solution.

The parameters k_f, F, $R_{1,f}$, $R_{1,r}$, $T_{2,f}$, and $T_{2,r}$ are not uniquely determined for experiments in the steady state (*32*). Following the approach of (*15*), we resolved this by making an independent measurement of the apparent relaxation rate R_1^{obs} and estimating $R_{1,r}$. In the absence of irradiation, a binary spin bath system can be expected to relax with the two spin–lattice relaxation rates. However, for typical inversion recovery experiments only the longer of the two can be observed. Hence, $R_{1,f}$ is related to R_1^{obs} by

$$R_{1,f} = \frac{R_1^{obs}}{1 + \left(\frac{\left[\frac{k_f}{R_{1,f}} \right] (R_{1,r} - R_1^{obs})}{(R_{1,r} - R_1^{obs}) + k_f/F} \right)}. \qquad [10]$$

$R_{1,r}$ was chosen rather arbitrarily to be 1 s^{-1} with an uncertainty, for the purpose of error calculations, of ± 1 s^{-1}. In practice, this has little impact on subsequent estimates of the other parameters.

R_1^{obs} was determined for each gel using a standard inversion recovery sequence with a TR of 2 s and a range of inversion times. Estimates were made using a nonlinear least-squares fit

to the data. For completeness the apparent T_2 of the gels was also measured using a 32-echo quantitative T_2 imaging sequence (*33*). All experiments were conducted at 1.5 T on a Siemens Vision scanner (Siemens Medical Systems, Erlangen).

2.6. Parameter Estimation

The material properties were estimated for each experiment by nonlinear least-squares fitting of the MTSPGR signal equation with $T_{2,f}$, $T_{2,r}$, k_f, and F as independent parameters. The corresponding value of $R_{1,f}$ for each parameter estimate was determined using Eq. [10] and the estimates of R_1^{obs} and $R_{1,r}$. In practice a scale factor could also be included as a free parameter in the fit; however, since the data are normalized, we fixed this scale factor for each parameter estimate such that the signal magnitude in the absence of MT pulses is one. This same technique was used to estimate the parameters used to generate the numerical simulations described in Section 2.4.

For the purposes of parameter estimation, one need not be restricted to data from a single type of experiment. We also estimated the material properties based on a simultaneous fit to data from all five experiment types. In principle the inversion recovery data used to estimate R_1^{obs} could also be included in a simultaneous fit to the MT data. However, the precision of the R_1^{obs} estimates was such that this added complication was deemed unnecessary.

For the experiments in which frequency offsets were encoded spatially, the number of measurements was too large to process easily. For these experiments the data were approximated using cubic B-splines and sampled regularly in logarithmic steps from 300 Hz to 80 kHz with 10 samples per decade. For the imaging experiments, which had comparatively few measurements, no resampling was done.

The MTP type experiments were analyzed using the same formula as for the MTSPGR experiments by taking the limit in which the excitation flip angle goes to zero. The analytic formula given by Henkelman *et al.* (*15*) for CW experiments can also be used to analyze the MTP type experiments. The two approaches differ in their handling of the free pool magnetization at small offset frequencies, where the simulation of the Bloch equations used in the MTSPGR signal equation differs from the Lorentzian lineshape approximation used in the CW equation. In practice, the two formulas agree closely for MTP experiments at offset frequencies greater than 1 kHz. However, the MTSPGR signal equation has the flexibility to take the duty cycle of the irradiation into account.

3. RESULTS

3.1 Numerical Simulations

In comparing the results of the ODE simulations to the predictions of our signal equations, we found the two to be generally in agreement. The residual differences, most noticeable for the 8% agar, followed a number of trends. At low-frequency offsets, from 100 Hz to 1 kHz, the signal equation consistently underestimates the simulation, likely as a result of the approximations used in modeling the free pool. This trend appears in all four cases shown in Fig. 1. Since the effect of decreasing $T_{2,f}$ is to shift the low-frequency portion of the curve to the right, one can expect this discrepancy to result in $T_{2,f}$ being overestimated. Parameters derived from simulations for each of the five experiment types were found to overestimate $T_{2,f}$ on average by 2 ms for each gel.

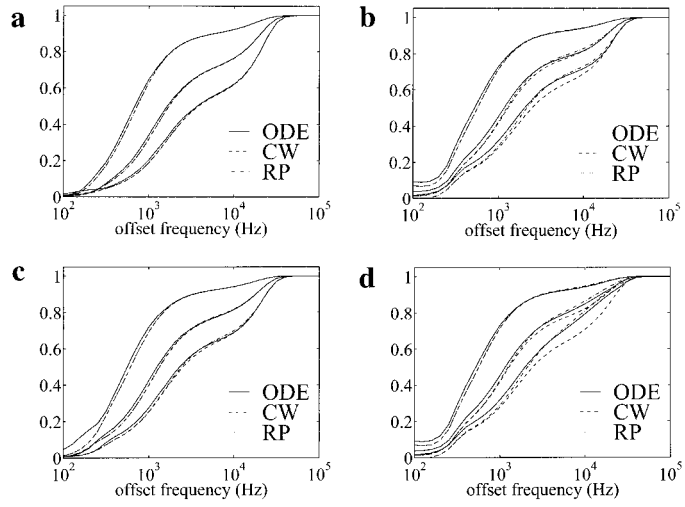

FIG. 1. Comparison of ODE solutions with two variants of the MTSPGR signal equation for 8% agar. The two variants use the continuous-wave (CW) and rectangular pulse (RP) approximations for the restricted pool. The three curves shown for each case correspond to the three MT pulse powers used throughout (see Table 2). (a) Experiment type 1, without dipole interaction (i.e., $T_D \to 0$). (b) Experiment type III, without dipole interaction. (c) Experiment type V, without dipole interaction. (d) Experiment type III, with dipole interaction ($T_D = 3$ ms).

In the range 1 kHz to 10 kHz off resonance, the deviation depended on both the variant of the signal equation and the type of experiment. In general, the rectangular pulse (RP) variant of the signal equation tended to slightly overestimate the signal in this range, while the continuous-wave variant would underestimate the signal by either a large or a small amount depending on the type of experiments. This latter trend is consistent with experiments having short relatively intense pulses deviating from the CW model. Compare, for example, the curves in Figs. 1a and 1b. The latter, a type III experiment, has less frequent and more intense pulses.

In the absence of dipole interaction (i.e., $T_D \to 0$), the two variants of the signal equation were in good agreement with the ODE simulation beyond 10 kHz. Incorporating dipole interaction increased the deviation of the CW model variant from the ODE solution. Compare, for example, Figs. 1b and 1d, where for the latter the curves only converge just before the MT effect disappears around 30 kHz.

3.2. Experimental Validation

For each agar gel and each experiment type we estimated the various material parameters by nonlinear least-squares fitting. On the basis of the numerical simulations of the previous section we restricted our analysis to the RP variant of the signal equation, looking at forms with and without the dipolar terms. The predictions of these two variants of the signal equation along with experimental data for an MTP and MTSPGR type experiment are shown in Fig. 2. While the parameter estimates derived from the two signal equations differ, the predicted signals are nearly identical except for small differences around 10 kHz for the MTSPGR experiment.

The RMS error for these fits is about 1% for the MTP experiment and 2% for the MTSPGR experiment. Much of the error in the latter is due to errors in the model for small frequency offsets. Considering only offset frequencies greater than 800 Hz, the RMS error for the MTSPGR experiment is about 1%. We restrict our attention to this range of offset frequencies since the signal change observed at smaller offset frequencies is almost entirely due to direct saturation and largely independent of the MT properties of the material. Furthermore, the large rotations of the spins in the free pool caused by pulses near resonance are difficult to model accurately. The low-frequency structure seen in the upper right panel of Fig. 2 is characteristic of pulsed MT experiments in which the fractional saturation of the free pool due to an individual pulse initially oscillates as the offset frequency is increased.

While these fits, as shown by Fig. 2, are generally close to the data, there are a number of systematic differences, statistically significant by a χ^2 test,[1] that are not accounted for by random variations. While these deviations could be attributed to deficiencies in the signal equation, measurement drift and B_1 inhomogeneity may also be the cause. The latter may account for the mismatch, seen in Fig. 2 at 8 kHz, between data collected for the three different ranges of offset frequencies, corresponding to the three gradient strengths.

To assess the effect of neglecting the dipole terms in the signal equation, we tested whether the difference between the resulting fitted curves was significant given the measurement noise. Using the test (*34*)

$$P\left\{ Z > \frac{1}{2\sigma} \sqrt{\sum_i \left(m_{\mathrm{dp}}(i) - m_z(i)\right)^2} \right\} < 1\%, \qquad [11]$$

we found in every case that the difference between the two was sufficient to choose the form with dipolar terms. $m_{\mathrm{dp}}(i)$ and $m_z(i)$ in Eq. [11] are the points on the fitted curve corresponding to the ith measurement for each signal equation and σ is the standard deviation of the measurement noise. The improvement in fits by including dipolar terms tended to be subtle, resulting on average in a 5% reduction in that portion of the residual error not accounted for by measurement noise.

We also investigated the effect of neglecting the dipole terms on the parameter estimates by comparing the estimates drawn from simultaneous fits of each model to all five experiment types for each gel. To assess the precision of these estimates we computed the marginal uncertainty for each parameter (*35*) using both the residual sum of squares error in the measurements and the uncertainties in R_1^{obs} and $R_{1,\mathrm{r}}$. Based on the gradient of the objective function for each measurement, this yields a t statistic with $N - p$ degrees of freedom and a corresponding confidence interval for the parameter. Since the parameter estimates are based on the resampled data, the fraction of the residual error due to systematic errors is correspondingly larger. As a result, the error bounds on the parameters reflect both the precision or reproducibility of the measurements and the accuracy of the model. These parameter estimates and corresponding uncertainties are given in Table 3. R_1^{obs} determined from inversion recovery experiments was 0.410 ± 0.006, 0.504 ± 0.02, and 0.699 ± 0.04 s^{-1}, respectively, for the 2, 4, and 8% agar gels.

Inspection of Table 3 would suggest that neglecting the dipole terms in the model results in a slight underestimate of the restricted pool size F and the exchange rate k_{f} as well as a small overestimate of $T_{2,\mathrm{r}}$. An analysis of variance of each parameter taking into account the large number of degrees of freedom in the individual entries reveals that only the reduction in F is statistically significant (tested at $p = 0.05$).

Note that $F/(1 + F)$ is expected to be proportional to the concentration of gel. Regressing the F values in Table 3 using this relation shows the average deviation for F to be 0.0017, somewhat larger than the reported uncertainty. Subsequent results show that such bias tends to be correlated with bias in k_{f} and $T_{2,\mathrm{f}}$.

We also investigated the effect of experimental design on the parameter estimates. In Fig. 3, parameter estimates are graphed for each experiment type and each gel using the MTSPGR signal equation including dipole terms. While these parameter estimates are generally in agreement with those derived from a simultaneous fit to all experiment types, we note that k_{f} and T_{D} are not well constrained for these fits, particularly for 2% agar. In addition, there is some disagreement among estimates of F that are matched by a reciprocal trend in the estimates of $T_{2,\mathrm{f}}$. An independent measurement of $T_{2,\mathrm{f}}$ using the multiecho T_2 sequence gave a T_2 of 70.1 ± 0.1, 38.5 ± 0.2, and 18.3 ± 3 ms for 2, 4, and 8% agar, respectively.

3.3. Parameter Images

For the imaging data we looked at both the accuracy of the estimates as compared to the nonimaging studies and the precision of the estimates as reflected by the within image variation. We computed estimates using both variants of the

[1] The statistic $\chi^2/(df - 1)$, where df is the number of degrees of freedom, averaged 45 for these fits, confirming the presence of systematic errors.

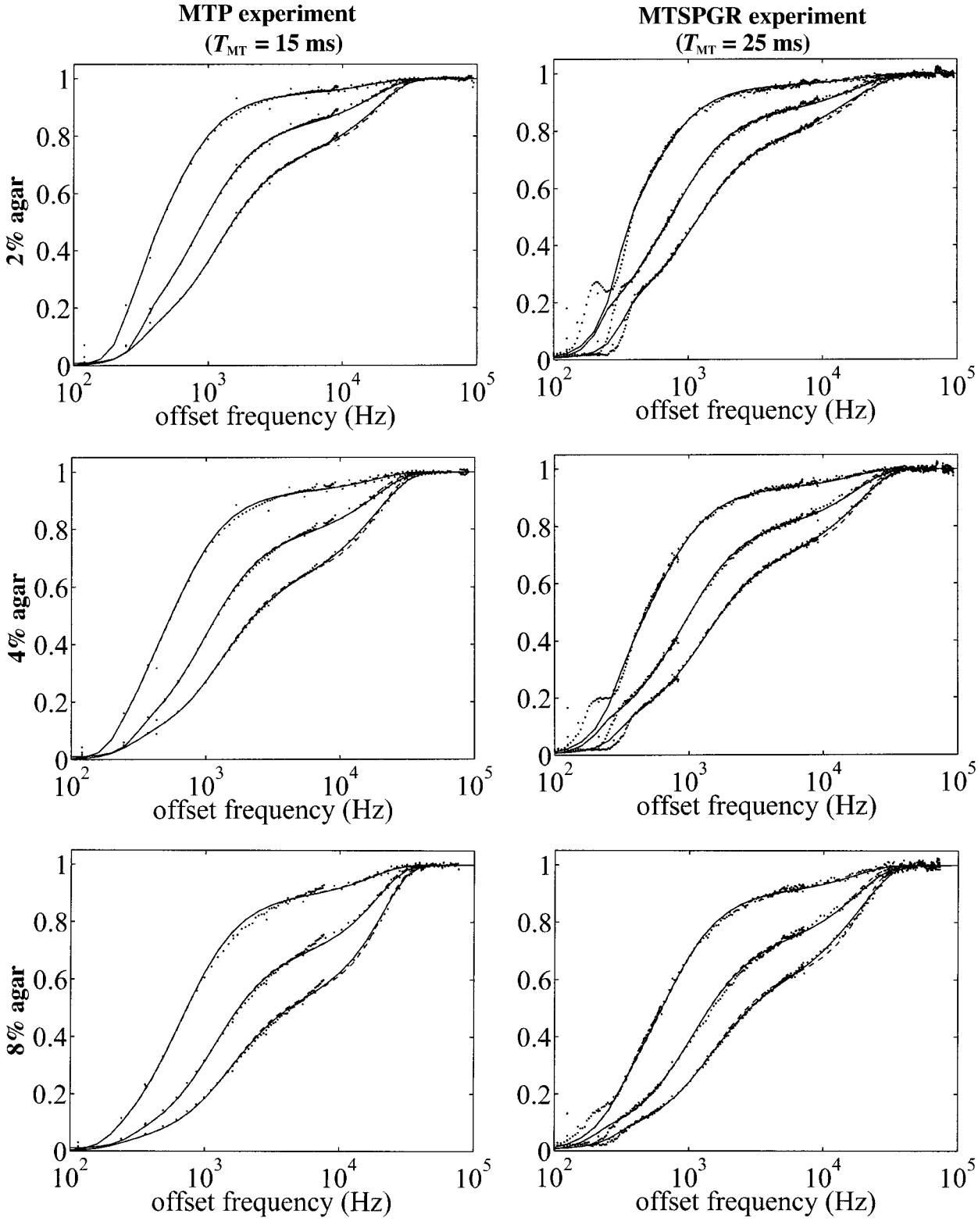

FIG. 2. Fitted curves for type I and type V experiments. Dots are experimental data; the solid and dashed lines are for the RP variant of the signal equation with and without dipole interaction, respectively. Note that the solid and dashed lines are indistinguishable in most plots.

TABLE 3
Parameter Estimates for Agar Gels Based on a Simultaneous Fit of the Signal Equation to the Five Experiments

		2% agar	4% agar	8% agar
k_f	[a]	$0.324 \pm 0.09\ s^{-1}$	$0.822 \pm 0.25\ s^{-1}$	$2.035 \pm 0.56\ s^{-1}$
	[b]	$0.313 \pm 0.08\ s^{-1}$	$0.784 \pm 0.23\ s^{-1}$	$1.895 \pm 0.52\ s^{-1}$
F	[a]	0.0092 ± 0.0011	0.0151 ± 0.0012	0.0302 ± 0.0016
	[b]	0.0087 ± 0.0009	0.0140 ± 0.0009	0.0274 ± 0.001
$R_{1,f}$	[a]	$0.405 \pm 0.01\ s^{-1}$	$0.497 \pm 0.022\ s^{-1}$	$0.690 \pm 0.049\ s^{-1}$
	[b]	$0.406 \pm 0.01\ s^{-1}$	$0.497 \pm 0.02\ s^{-1}$	$0.691 \pm 0.05\ s^{-1}$
$R_{1,r}$	[a]	$1.0 \pm 1.0\ s^{-1}$	$1.0 \pm 1.0\ s^{-1}$	$1.0 \pm 1.0\ s^{-1}$
	[b]	$1.0 \pm 1.0\ s^{-1}$	$1.0 \pm 1.0\ s^{-1}$	$1.0 \pm 1.0\ s^{-1}$
$T_{2,f}$	[a]	54.4 ± 1.3 ms	31.8 ± 0.9 ms	16.7 ± 0.3 ms
	[b]	54.2 ± 1.3 ms	31.5 ± 0.9 ms	16.5 ± 0.3 ms
$T_{2,r}$	[a]	$13.8 \pm 1.2\ \mu s$	$13.7 \pm 0.8\ \mu s$	$13.6 \pm 0.5\ \mu s$
	[b]	$14.4 \pm 0.9\ \mu s$	$14.6 \pm 0.6\ \mu s$	$14.5 \pm 0.4\ \mu s$
T_D	[a]	0.3 ± 0.5 ms	0.5 ± 0.4 ms	0.6 ± 0.3 ms
	[b]			

Note. Values are shown for a model with and without dipole interaction. Uncertainties are for a 95% confidence interval.
[a] Signal equation with dipolar terms.
[b] Signal equation without dipolar terms.

model by simultaneously fitting the type IV and type V data as well as by fitting the type V alone. Parameter images derived from the simultaneous fit of the model without dipole terms are shown in Fig. 4. Also shown are intensity profiles taken along a line in the F and k_f images. These images show good uniformity, as a result of compensation for excitation field and reception sensitivity variations, as well as good SNR.

We evaluated the precision of these estimates by computing the standard deviation within regions of interest corresponding to the four bottles. These regions were defined by thresholding the image and eroding the resulting mask by one voxel. The mean and standard deviation for each bottle and each parameter are given in Table 4 for the simultaneous fits. The results of fitting to the type V experimental data alone proved highly unstable and are not shown.

Comparing the parameter estimates for the two variants of the model shows that the two are largely in agreement with subtle difference following the same trend as for the nonimaging experiments. However, variability in the estimates of k_f for the model including dipole interaction is significantly higher than that without. In addition, the variations in T_D suggest that it is not well constrained by this experimental design. Comparing the parameter estimates with those of the nonimaging experiments shows that the estimates of F are consistently lower and the estimates of k_f are consistently higher for the imaging experiments.

4. DISCUSSION

The goal of this work was to demonstrate the feasibility of using conventional MT-weighted MRI pulse sequences to rapidly produced quantitative images of the exchange and relaxation properties within an object. To describe these properties

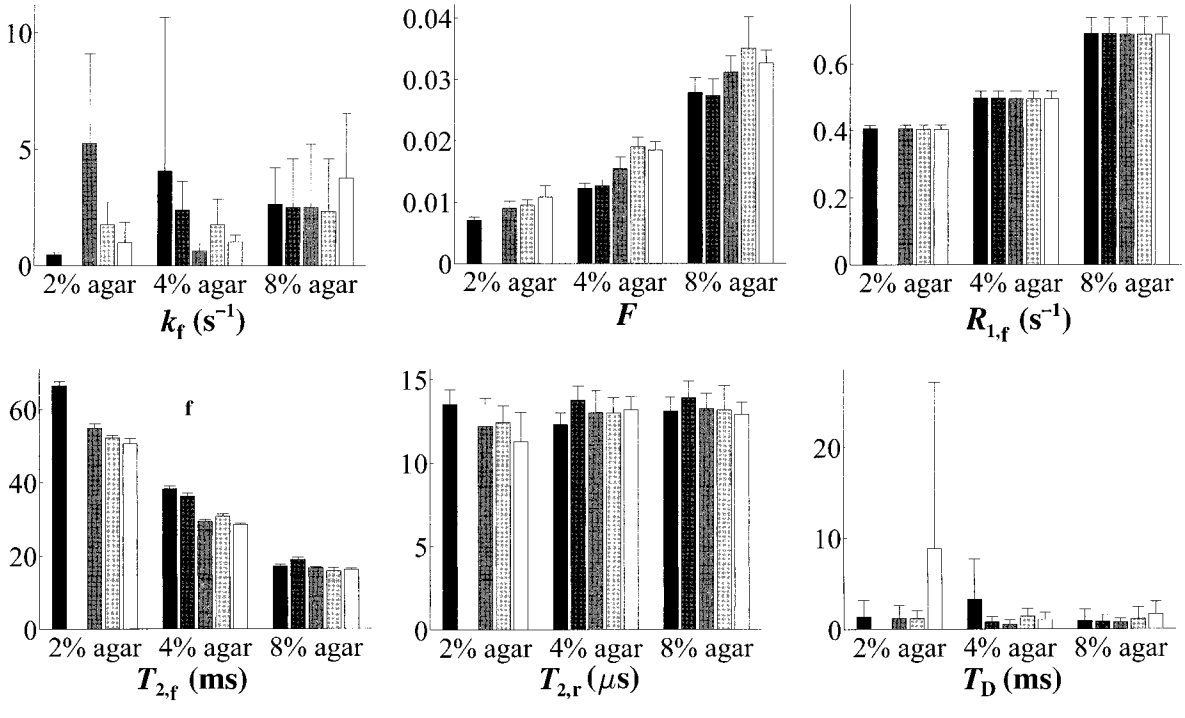

FIG. 3. Comparison of parameter estimates for various experimental designs. The five bars for each gel correspond to experiment types I through V. Error bars form a 95% confidence interval. Type II experimental data for 2% agar is not available and intentionally left blank.

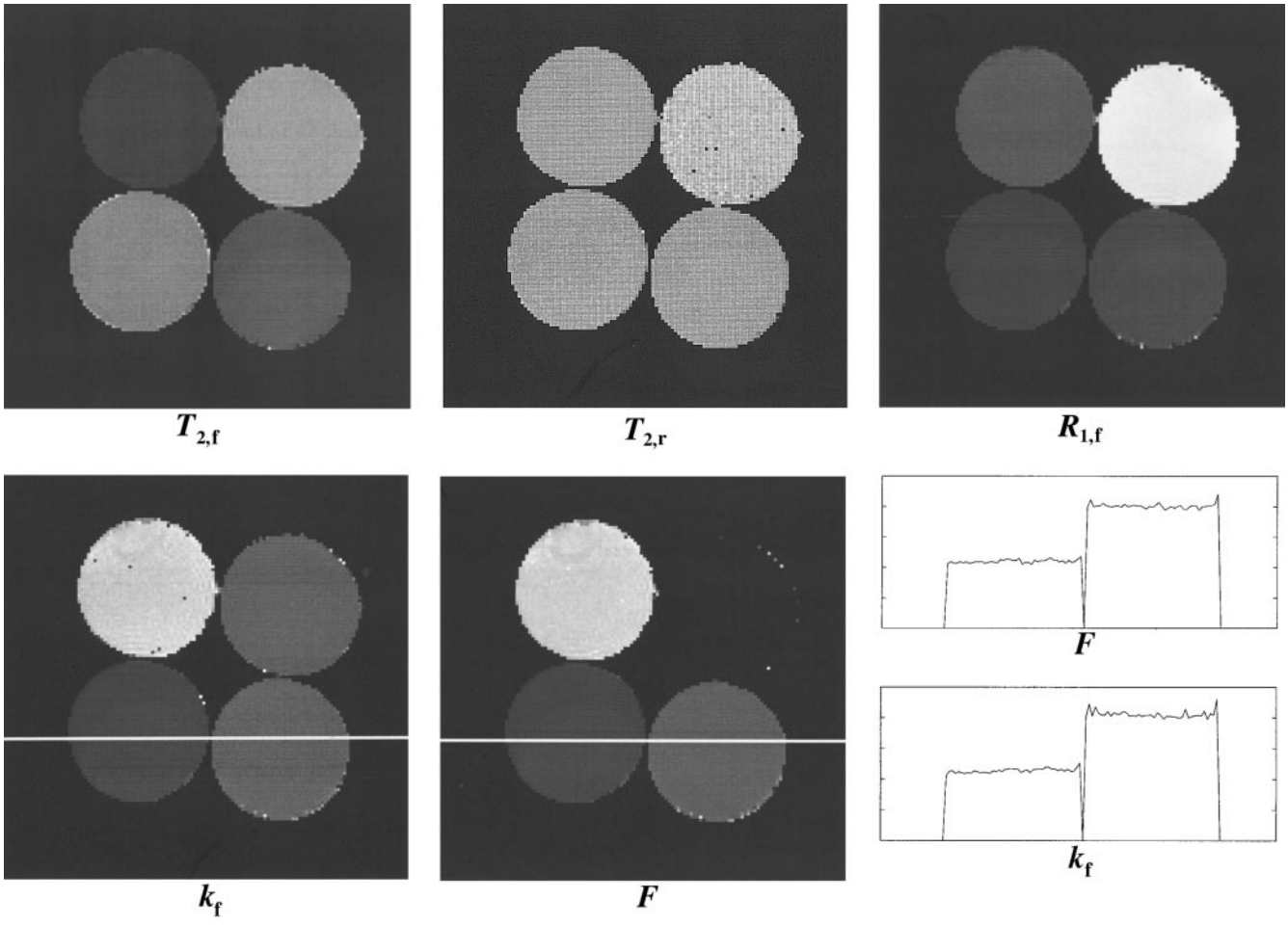

FIG. 4. Parameter images based on a simultaneous fit of type IV and type V experiments using the RP variant of the MTSPGR signal equation neglecting dipole interaction. The materials shown, moving clockwise from the top left, are 8% agar, $MnCl_2$ solution, 4% agar, and 2% agar. Also shown are profiles across the F and k_f parameter maps.

we have employed the binary spin bath model with a Gaussian lineshape. While this model well characterizes the gels used in our studies, there are a number of considerations in generalizing this technique to *in vivo* studies. A number of authors have described alternate lineshapes that are more suitable for tissue (*21*, *36*, *37*). Also, there is some evidence that tissues such as white matter are better characterized by a model with two free water (long T_2) components (*38–40*). While changing the lineshape is straightforward it is not clear whether adding additional compartments to the model will be beneficial. The situation may prove to be similar to our results with adding dipolar terms to the model, in which improvements in accuracy are offset by a loss of precision through greater sensitivity to noise. For completeness, the binary spin bath model should also allow for exchange of transverse magnetization (*41*). However, we found that in ODE simulations of our experiments this effect is negligible.

In implementing the MTSPGR signal equation, we considered both a continuous-wave (CW) and a rectangular pulse (RP) approximation for the restricted pool. While the CW approximation was satisfactory for experiments in which the duty cycle of pulsation was large, it proved inadequate at small duty cycles. This is because the time constant for equilibration of the two pools is on the order of a few milliseconds, comparable with the duration of the MT pulses. The RP approximation, by taking into account the duty cycle and pulsation frequency, offers extra freedom in designing experiments, which can be used to advantage in improving estimates of the exchange constant k_f. In particular, we found that for imaging studies, including experimental data from two different pulse sequences improved the estimates of k_f beyond what could expected from an equivalent increase in SNR.

In choosing a signal equation, we tried to establish whether including dipolar terms in the model improved the parameter estimates. The results of our nonimaging studies show that the dipolar terms make a statistically significant improvement in the fit of the model and that neglecting the dipolar terms results in a modest underestimate of the pool size fraction F. However, we also found that neglecting the dipolar terms substantially improved the precision of the estimates of k_f in the

TABLE 4
Parameter Estimates for Agar Gels Averaged over Each Region of the Parameter Maps

		$MnCl_2$	2% agar	4% agar	8% agar
k_f	[a]		$0.842 \pm 0.2\ s^{-1}$	$1.37 \pm 0.3\ s^{-1}$	$2.47 \pm 1\ s^{-1}$
	[b]		$0.734 \pm 0.05\ s^{-1}$	$1.32 \pm 0.2\ s^{-1}$	$2.78 \pm 0.3\ s^{-1}$
F	[a]	0	0.0074 ± 0.0016	0.0121 ± 0.001	0.0271 ± 0.004
	[b]	0	0.0066 ± 0.0004	0.0121 ± 0.002	0.0260 ± 0.002
$R_{1,f}$	[a]	$2.07 \pm 0.05\ s^{-1}$	$0.419 \pm 0.002\ s^{-1}$	$0.483 \pm 0.1\ s^{-1}$	$0.760 \pm 0.04\ s^{-1}$
	[b]	$2.07 \pm 0.05\ s^{-1}$	$0.419 \pm 0.02\ s^{-1}$	$0.483 \pm 0.1\ s^{-1}$	$0.760 \pm 0.04\ s^{-1}$
$R_{1,r}$	[a]		$1.0 \pm 1.0\ s^{-1}$	$1.0 \pm 1.0\ s^{-1}$	$1.0 \pm 1.0\ s^{-1}$
	[b]		$1.0 \pm 1.0\ s^{-1}$	$1.0 \pm 1.0\ s^{-1}$	$1.0 \pm 1.0\ s^{-1}$
$T_{2,f}$	[a]	66.8 ± 3 ms	57.3 ± 3 ms	33.8 ± 3 ms	16.8 ± 1 ms
	[b]	66.8 ± 3 ms	56.4 ± 3 ms	33.7 ± 2 ms	16.8 ± 0.9 ms
$T_{2,r}$	[a]		13.1 ± 2 μs	14.1 ± 0.6 μs	14.1 ± 1 μs
	[b]		14.3 ± 0.5 μs	14.1 ± 0.3 μs	14.1 ± 0.3 μs
T_D	[a]		1.32 ± 3 ms	0.02 ± 0.5 ms	0.14 ± 1 ms
	[b]				

[a] Signal equation with dipolar terms.
[b] Signal equation without dipolar terms.

imaging experiments. Hence, there is a trade-off between accuracy and precision when including the dipolar terms in the model which favors neglecting them. One cannot generalize this conclusion to other materials, however, since the uncertainty in k_f tends to decrease as F increases and k_f decreases.

There are a number of factors to consider in designing an experiment. In particular, the range of offset frequencies, average irradiation powers, and pulse repetition periods to sample needs to be selected. While we did not consider all of these factors in detail, we noted a number of trends. With respect to pulses powers, we found little benefit in choosing more than two pulse powers for an experiment beyond that which can be expected from an equivalent number of repeated measurements. For this reason, in the imaging experiments the number of pulse angles was reduced from 3 to 2. With respect to frequency offsets, there is clearly little benefit in sampling offsets so close to resonance that the free pool is saturated or so far from resonance that the MT effect disappears. Intuitively, one would expect that offsets at which the MT effect or *bite* is largest to be the most useful (2 through 20 kHz for the agar gels considered here); however, taking advantage of this would require a priori knowledge of the linewidth. Since the duration of the pulses is comparable to the equilibration time for the two pools, the behavior of a sequence depends on both the pulse duration and the interpulse interval for a given average power. We found that sampling more than one of these combinations substantially improved the estimates of k_f.

Besides optimizing the sampling, a variety of fast imaging techniques could be employed to speed up the data acquisition. The MTSPGR sequence with TR = 50 ms, 128 phase encodes, 8 signal averages, and 12.8 s of preparation takes 64 s per sample image. This sequence easily generalizes to 3D by exchanging signal averages for phase encode steps in the slice direction with little increase in total scan time. Alternately, one can use an MTP type sequence and collect an image in a single shot following the preparatory pulsing. Similar modification can be made to reduce the imaging time required to collect B_0, B_1, and R_1^{obs} data. Given these fast imaging modifications to the pulse sequences, single slice imaging would be feasible within a clinically acceptable scan time of perhaps 30 min and likely multislice imaging would be as well.

While the results of our experiments were generally in agreement with those reported in (*15*) (see Table 1), the discrepancies exceed the quoted uncertainties. In particular, R_1^{obs} differs significantly between the two sets of experiments. Since this parameter is determined in a separate inversion recovery experiment and influences the subsequent estimate of the other parameters, the differences between the results may be due to this factor alone. Given that there may also be differences between gel preparations, we looked at the consistency of results between the different experiments we performed on the same gel in assessing experimental accuracy.

The results of the imaging experiments were generally in agreement with the results of the nonimaging experiments; however, we did note systematic differences in the estimates of F and k_f. In general, we found that the uncertainty in F and k_f was correlated such that underestimates of F were matched by overestimates of k_f. A similar correlation was observed between F and $T_{2,f}$. As seen from the parameter estimates for the individual experiment types in Fig. 3, each experiment has a different bias in this respect. We attribute these biases to subtle differences between the approximations in the signal equation and the putatively correct ODE solution. Since these differences are smallest for pulsation that resembles continuous-wave irradiation one might expect pulse sequences with frequent pulses to be more accurate. However, since we found that the k_f parameter is not well constrained by this kind of experiment alone, such a solution is unsatisfactory. In practice,

one may prefer a design with some inherent bias to gain greater precision in repeated measurements.

5. CONCLUSION

We have described a method for analyzing general pulsed MT experiments in which the magnetization is driven to steady state. From experiments on agar gel, we have shown that this method can be used to reliably and accurately estimate the exchange and relaxation properties of a material in an imaging context. Such an approach offers advantages over imaging techniques yielding magnetization transfer contrast ratios both from the perspective of providing more information and for being comparable among different pulse sequences and scanning hardware. While minor changes in the model are needed to account for the differences between agar gel and tissue, our results indicate that it is feasible to use this technique *in vivo.*

APPENDIX

The solutions for the steady-state magnetization of an MTSPGR experiment can be computed as follows. Equations [1]–[5] can be written in matrix form as

$$\frac{\mathbf{M}(t)}{dt} = \mathbf{A}(t)\mathbf{M}(t) + \mathbf{B}\mathbf{M}_0, \qquad [A1]$$

where $\mathbf{M}$ is a magnetization vector, $\mathbf{M}_0$ is the fully relaxed state of the magnetization, and $\mathbf{A}$ and $\mathbf{B}$ are matrices corresponding to the coefficients of Eqs. [1]–[5]. Approximating a pulse sequence as a series of periods of free precession (fp), continuous-wave irradiation (cw) of the restricted pool, or instantaneous saturation (is) of the free pool, the matrix $\mathbf{A}$ is constant for each of these periods. Since the transverse magnetization of the free pool is decoupled from the other components in each of these cases, only the longitudinal components are used for computation and the transverse components are assumed to disappear through relaxation and spoiling. The state of the magnetization after a period τ for each of these cases is notated $F_*(M, \tau)$ and given by

$$F_{\text{fp}}(\mathbf{M}, \tau) = e^{-\mathbf{A}_{\text{fp}}\tau}\mathbf{M} + [\mathbf{I} - e^{-\mathbf{A}_{\text{fp}}\tau}]\mathbf{M}_0 \qquad [A2]$$

$$F_{\text{cw}}(\mathbf{M}, \tau) = e^{-\mathbf{A}_{\text{cw}}\tau}\mathbf{M} + [\mathbf{I} - e^{-\mathbf{A}_{\text{cw}}\tau}]\mathbf{M}_{\text{cw}}^{\text{ss}} \qquad [A3]$$

$$F_{\text{is}}(\mathbf{M}) = \mathbf{S}\mathbf{M}. \qquad [A4]$$

$\mathbf{S}$ is a diagonal matrix with elements $[S_{\text{f}}\ 1\ 1]$, where S_{f} is the fractional saturation of the free pool due to the given pulse. S_{f} is computed by solving for the magnetization of the free pool following the given pulse using Eqs. [1] and [2] with $R_{1,\text{f}}$, k_{f}, and k_{r} equal to zero and the initial condition $\mathbf{M} = \mathbf{M}_0$. The ratio of $M_{z,\text{f}}$ before and after the pulse is S_{f}.

$\mathbf{M}_{\text{cw}}^{\text{ss}}$ is the steady state of the magnetization established after a long period of continuous-wave irradiation of the restricted pool:

$$\mathbf{M}_{\text{cw}}^{\text{ss}} = \begin{bmatrix} \dfrac{M_{0,\text{f}}(R_{1,\text{r}}k_{\text{f}} + R_{1,\text{r}}R_{1,\text{f}} + R_{1,\text{f}}k_{\text{r}} + WR_{1,\text{f}})}{R_{1,\text{r}}R_{1,\text{f}} + R_{1,\text{r}}k_{\text{f}} + R_{1,\text{f}}k_{\text{r}} + WR_{1,\text{f}} + Wk_{\text{f}}} \\ \dfrac{M_{0,\text{r}}(R_{1,\text{r}}R_{1,\text{f}} + R_{1,\text{r}}k_{\text{f}} + R_{1,\text{f}}k_{\text{r}})}{R_{1,\text{r}}R_{1,\text{f}} + R_{1,\text{r}}k_{\text{f}} + R_{1,\text{f}}k_{\text{r}} + WR_{1,\text{f}} + Wk_{\text{f}}} \end{bmatrix}. \qquad [A5]$$

Using these equations one can solve for the steady-state magnetization of a periodic pulse sequence using the relation

$$\mathbf{M}(t + \text{TR}) = \mathbf{M}(t). \qquad [A6]$$

For example, a period from a simplified version of the MTSPGR sequence could be described in three steps: instantaneous saturation of the free pool due to the MT pulse, instantaneous saturation of the free pool by the excitation pulse, and a period of continuous-wave irradiation of the restricted pool of duration TR. Combining these yields the equation

$$\mathbf{M} = F_{\text{cw}}(\mathbf{S}_2\mathbf{S}_1\mathbf{M}, \text{TR}), \qquad [A7]$$

where $\mathbf{S}_1$ and $\mathbf{S}_2$ are fractional saturation matrices due to the MT and excitation pulses, respectively.

The observed magnetization $M_{xy,\text{f}}$ is given by

$$M_{xy,\text{f}} = cS_{1,\text{f}}M_{z,\text{f}}^{\text{ss}}\sin\theta, \qquad [A8]$$

where θ is the flip angle of the excitation pulse and c is a constant reflecting other factors such as proton density and equipment sensitivity. Solving Eqs. [A7] and substituting the result into [A8] yields for the case of ($T_{\text{D}} \rightarrow 0$) after some simplification

$$M_{xy,\text{f}} = \frac{c(E_1 - 1)(E_2 - 1)(\lambda_2 - \lambda_1)S_{1,\text{f}}M_{z,\text{f}}^{\text{ss}}\sin\theta}{(E_1 - 1)(S_{\text{f}}E_2 - 1)(\lambda_2 - \lambda_1) + (S_{\text{f}} - 1)(E_2 - E_1)(\lambda_2 - R_{1,\text{f}} - k_{\text{f}})}, \qquad [A9]$$

where $\lambda_{1,2}$ are the eigenvalues of $\mathbf{A}_{\text{cw}}$ given by

$$\lambda_{1,2} = \tfrac{1}{2}(R_{1,\text{f}} + k_{\text{f}} + R_{1,\text{r}} + k_{\text{r}} + W) \pm \tfrac{1}{2}\sqrt{(R_{1,\text{f}} + k_{\text{f}} + R_{1,\text{r}} + k_{\text{r}} + W)^2 - 4(R_{1,\text{f}}R_{1,\text{r}} + k_{\text{f}}R_{1,\text{r}} + R_{1,\text{f}}k_{\text{r}} + R_{1,\text{f}}W + k_{\text{f}}W)}$$

with $E_1 = e^{-\lambda_1 t}$ and $E_2 = e^{-\lambda_2 t}$.

For the RP variant of the MTSPGR signal equation the approximate pulse sequence has the following steps: instantaneous saturation of the free pool from the MT and excitation pulse, continuous-wave irradiation of the restricted pool for a period $\tau/2$, a period TR $-$ τ of free precession,

and finally another period of continuous-wave irradiation of duration $\tau/2$. Combining all of these steps and solving for **M** as before yields an expression for the steady-state magnetization that is, while cumbersome to write out in full, straightforward to compute.

ACKNOWLEDGMENTS

This work was supported by the Natural Sciences and Engineering Research Council of Canada, the Medical Research Council of Canada, Fonds de la Recherche en Santé du Québec, and the Killam Foundation.

REFERENCES

1. S. D. Wolff and R. S. Balaban, Magnetization transfer contrast (MTC) and tissue water proton relaxation *in vivo, Magn. Reson. Med.* **10,** 135–144 (1989).
2. S. D. Wolff, J. Eng, and R. S. Balaban, Magnetization transfer contrast: Method for improving contrast in gradient-recalled-echo images, *Radiology* **179,** 133–137 (1991).
3. R. J. Ordidge, R. A. Knight, and J. A. Helpern, Magnetization transfer contrast (MTC) in flash MR imaging, *Magn. Reson. Imaging* **9,** 889–893 (1991).
4. J. V. Hajnal, C. J. Baudouin, A. Oatridge, I. R. Young, and G. M. Byddder, Design and implementation of magnetization transfer pulse sequences for clinical use, *J. Comput. Assist. Tomogr.* **16,** 7–18 (1992).
5. G. B. Pike, B. S. Hu, G. H. Glover, and D. R. Enzmann, Magnetization transfer time-of-flight magnetic resonance angiography, *Magn. Reson. Med.* **25,** 372–379 (1992).
6. I. Berry, G. J. Barker, F. Barkhof, A. Campi, V. Dousset, J. M. Franconi, A. Gass, W. Schreiber, D. H. Miller, and P. S. Tofts, A multicenter measurement of magnetization transfer ratio in normal white matter, *J. Magn. Reson. Imaging* **9,** 441–446 (1999).
7. J. Eng, T. I. Ceckler, and R. S. Balaban, Quantitative ^{1}H magnetization transfer imaging *in vivo, Magn. Reson. Med.* **17,** 304–314 (1991).
8. H. N. Yeung, R. S. Adler, and S. D. Swanson, Transient decay of longitudinal magnetization in hetrogeneous spin systems under selective saturation. IV. Reformulation of the spin-bath-model equations by the Redfield–Provotorov theory, *J. Magn. Reson. A* **106,** 37–45 (1994).
9. C. Morrison, G. Stanisz, and R. M. Henkelman, Modeling magnetization transfer for biological-like systems using a semi-solid pool with a super-Lorentzian lineshape and dipolar reservoir, *J. Magn. Reson. B* **108,** 103–113 (1995).
10. H. T. Edzes and E. D. Samulski, Cross relaxation and spin diffusion in the proton NMR of hydrated collagen, *Nature* **265,** 521–523 (1977).
11. H. T. Edzes and E. D. Samulski, The measurement of cross-relaxation effects in the proton NMR spin–lattice relaxation of water in biological systems: Hydrated collagen and muscle, *J. Magn. Reson.* **31,** 207–229 (1978).
12. R. A. Hoffman, Transient and steady-state Overhauser experiments in the investigation of relaxation processes. Analogies between chemical exchange and relaxation, *J. Chem. Phys.* **45** (1966).
13. B. Quesson, E. Thiaudiere, C. Delalande, V. Dousset, J. F. Chateil, and P. Canioni, Magnetization transfer imaging in vivo of the rat brain at 4.7 T: Interpretation using a binary spin-bath model with a superlorentzian lineshape, *Magn. Reson. Med.* **38,** 974–980 (1997).
14. B. Quesson, E. Thiaudiere, C. Delalande, J. F. Chateil, C. T. W. Moonen, and P. Canioni, Magnetization transfer imaging of rat brain under non-steady-state conditions. Contrast prediction using a binary spin-bath model and a super-Lorentzian lineshape, *J. Magn. Reson.* **130,** 321–328 (1998).
15. R. M. Henkelman, X. Huang, Q. S. Xiang, G. J. Stanisz, S. D. Swanson, and M. J. Bronskill, Quantitative interpretation of magnetization transfer, *Magn. Reson. Med.* **29,** 759–766 (1993).
16. R. R. Lee and A. P. Dagher, Low power method for estimating the magnetization transfer bound-pool macromolecular fraction, *J. Magn. Reson. Imaging* **7,** 913–917 (1997).
17. J. W. Chai, C. Chen, J. H. Chen, S. K. Lee, and H. N. Yeung, Estimation of in vivo proton intrinsic and cross-relaxation rate in human brain, *Magn. Reson. Med.* **36,** 147–152 (1996).
18. D. F. Gochberg, R. P. Kennan, M. D. Robson, and J. C. Gore, Quantitative imaging of magnetization transfer using multiple selective pulses, *Magn. Reson. Med.* **41,** 1065–1072 (1999).
19. M. Goldman, "Spin Temperature and Nuclear Magnetic Resonance in Solids," Oxford Univ. Press, London (1970).
20. J. Listerud, Off-resonance pulsed magnetization transfer in clinical mr imaging: Optimization by an analysis of transients, *Magn. Reson. Med.* **37,** 693–705 (1997).
21. J. G. Li, S. J. Graham, and R. M. Henkelman, A flexible magnetization transfer line shape derived from tissue experimental data, *Magn. Reson. Med.* **37,** 866–871 (1997).
22. S. J. Graham and R. M. Henkelman, Quantifying the magnetization transfer produced by RF irradiation with multiple frequency components, *in* "Proc. 4th Int. Soc. Magn. Reson. Med., Vol. 1, p. 469 (1996).
23. S. J. Graham and R. M. Henkelman, Understanding pulsed magnetization transfer, *J. Magn. Reson. Imaging* **7,** 903–912 (1997).
24. G. Bodenhausen, H. Kogler, and R. R. Ernst, Selection of coherence-transfer pathways in NMR pulse experiments, *J. Magn. Reson.* **58,** 370–388 (1984).
25. G. B. Pike, Pulsed magnetization transfer contrast in gradient echo imaging: A two-pool analytic description of signal response, *Magn. Reson. Med.* **36,** 95–103 (1996).
26. Y. Zur, M. L. Wood, and L. J. Neuringer, Spoiling of transverse magnetization in steady-state sequences, *Magn. Reson. Med.* **21,** 251–263 (1991).
27. S. D. Swanson, Broadband excitation and detection of cross-relaxation NMR spectra, *J. Magn. Reson.* **95,** 615–618 (1991).
28. J. G. Sled and G. B. Pike, Standing-wave and RF penetration artifacts caused by elliptic geometry: An electrodynamic analysis of MRI, *IEEE Trans. Med. Imaging* **17,** 653–662 (1998).
29. J. G. Sled, A. P. Zijdenbos, and A. C. Evans, A non-parametric method for automatic correction of intensity non-uniformity in MRI data, *IEEE Trans. Med. Imaging* **17,** 87–97 (1998).
30. G. Glover and E. Schneider, Three-point Dixon technique for true water/fat decomposition with B_0 inhomogeneity correction, *Magn. Reson. Med.* **18,** 371–383 (1991).
31. S. Topp, E. Adalsteinsson, and D. M. Spielman, Fast multislice B_1-mapping, *in* "Proc. 5th Int. Soc. Magn. Reson. Med.," Vol. 1, p. 281 (1997).
32. G. H. Caines, T. Schleich, and J. M. Rydzewski, Incorporation of magnetization transfer into the formalism for rotating-frame spin–lattice NMR relaxation in the presence of an off-resonance-irradiation field, *J. Magn. Reson.* **95,** 558–566 (1991).

33. C. S. Poon and R. M. Henkelman, Practical T_2 quantitation for clinical applications, *J. Magn. Reson. Imaging* **2,** 541–553 (1992).

34. D. S. Borowiak, "Model Discrimination for Nonlinear Regression Models," Dekker, New York (1989).

35. D. M. Bates and D. G. Watts, "Nonlinear Regression Analysis and Its Applications," Wiley, New York (1988).

36. M. Iino, Transition from Lorentzian to Gaussian line shape of magnetization transfer spectrum in bovine serum albumin solutions, *Magn. Reson. Med.* **32,** 459–463 (1994).

37. C. Morrison and R. M. Henkelman, A model for magnetization transfer in tissues, *Magn. Reson. Med.* **33,** 475–482 (1995).

38. R. Harrison, M. J. Bronskill, and R. M. Henkelman, Magnetization transfer and T_2 relaxation components in tissue, *Magn. Reson. Med.* **33,** 490–496 (1995).

39. G. J. Stanisz, A. Kecojevic, M. J. Bronskill, and R. M. Henkelman, Characterizing white matter with magnetization transfer and T_2, *Magn. Reson. Med.* **42,** 1128–1136 (1999).

40. A. MacKay, K. Whittall, J. Adler, D. Li, D. Paty, and D. Graeb, In vivo visualization of myelin water in brain by magnetic resonance, *Magn. Reson. Med.* **31,** 673–677 (1994).

41. X. Wu and J. J. Listinsky, Effects of transverse cross relaxation on magnetization transfer, *J. Magn. Reson. B* **105,** 73–76 (1994).